**Atmospheric
Chemistry
and Physics
Discussions**

Assimilation of ground versus lidar observations for PM$_{10}$ forecasting

Y. Wang[1,2], K. N. Sartelet[1], M. Bocquet[1,3], and P. Chazette[2]

[1]CEREA, joint laboratory Ecole des Ponts ParisTech – EDF R&D, Université Paris-Est,
77455 Champs sur Marne, France
[2]LSCE, joint laboratory CEA – CNRS, UMR8212, 91191 Gif-sur-Yvette, France
[3]INRIA, Paris-Rocquencourt Research Center, Le Chesnay, France

Correspondence to: Y. Wang (wangy@cerea.enpc.fr)

Discussion Paper | Discussion Paper | Discussion Paper | Discussion Paper

ACPD

12, 23291–23331, 2012

Data assimilation

Y. Wang et al.

Title Page

Abstract	Introduction
Conclusions	References
Tables	Figures

◀◀ ▶▶

◀ ▶

Back Close

Full Screen / Esc

Printer-friendly Version

Interactive Discussion

Abstract

This article investigates the potential impact of future ground-based lidar networks on analysis and short-term forecasts of particulate matter with a diameter smaller than $10 \, \mu g \, m^{-3}$ (PM_{10}). To do so, an Observing System Simulation Experiment (OSSE) is
⁵ built for PM_{10} data assimilation (DA) using optimal interpolation (OI) over Europe for one month in 2001. First, using a lidar network with 12 stations, we estimate the efficiency of assimilating the lidar network measurements in improving PM_{10} concentration analysis and forecast. It is compared to the efficiency of assimilating concentration measurements from the AirBase ground network, which includes about 500 stations in
¹⁰ Western Europe. It is found that assimilating the lidar observations decreases by about 54 % the root mean square error (RMSE) of PM_{10} concentrations after 12 h of assimilation and during the first forecast day, against 59 % for the assimilation of AirBase measurements. However, the assimilation of lidar observations leads to similar scores as AirBase's during the second forecast day. The RMSE of the second forecast day is
¹⁵ improved on average over the summer month by 57 % by the lidar DA, against 56 % by the AirBase DA. Moreover, the spatial and temporal influence of the assimilation of lidar observations is larger and longer. The results show a potentially powerful impact of the future lidar networks. Secondly, since a lidar is a costly instrument, a sensitivity study on the number and location of required lidars is performed to help defining an
²⁰ optimal lidar network for PM_{10} forecast. With 12 lidar stations, an efficient network in improving PM_{10} forecast over Europe is obtained by regularly spacing the lidars. DA with a lidar network of 26 or 76 stations is compared to DA with the previously-used lidar network. The assimilation of 76 lidar stations' measurements leads to a better score than AirBase's during the forecast days.

1   Introduction

Aerosols have an impact on regional and global climates (Ramanathan et al., 2001; Léon et al., 2002; Sheridan et al., 2002; Intergovernment Panel on Climate Control, IPCC 2007) as well as on ecological equilibrium (Barker and Tingey, 1992) and hu-
5   man health by penetrating the respiratory system and leading to respiratory and cardiovascular diseases (Lauwerys, 1982; Dockery and Pope, 1996). Aerosols influence gaseous molecules photo-dissociation (Randriamiarisoa et al., 2004) and can thus have a significant impact on the photo-oxidant pollution (Dickerson et al., 1997). Thus the accurate prediction of aerosol concentration levels has signification human and
10 economic cost implications.

Various chemistry transport models are used to simulate or predict aerosol concentrations over Europe, e.g. EMEP (European Monitoring and Evaluation Programme) (Simpson et al., 2003), LOTOS (Long Term Ozone Simulation) – EUROS (European Operational Smog) (Schaap et al., 2004), CHIMERE (Hodzic et al., 2006), DEHM
15 (Danish Eulerean Hemispheric Model) (Brandt et al., 2007) and Polyphemus (Sartelet et al., 2007). However, uncertainties in modelling atmospheric components, in particular aerosols are high (Roustan et al., 2010), which leads to substantial discrepancies to observational data (Sartelet et al., 2007). Data assimilation (DA hereafter) can reduce the uncertainties in input data such as the initial conditions or the boundary conditions
20 by coupling models to observations (Bouttier and Courtier, 2001). In meteorology, DA has been traditionally applied to improve forecasts (Kalnay et al., 2003; Lahoz et al., 2010). In air quality, applications of DA to PM_{10} forecast are still sparse. They include Tombette et al. (2009) and Denby et al. (2008) over Europe and Pagowski et al. (2010) over the United States of America. They demonstrated the feasibility and the useful-
25 ness of DA for aerosol forecasts.

As in Tombette et al. (2009), in situ surface measurements are often assimilated, e.g. AirBase, BDQA (Base de Données de la Qualité de l'Air) or EMEP. However, they do not provide information on vertical profiles. Niu et al. (2008) used both satellite retrieval

data and surface observations to assimilate dust for sand and dust storm (SDS) forecasts. They found that information on the vertical profiles of the SDS was needed for the DA system. Although satellite passive remote sensing can provide vertical observations, it is very expensive and data are often limited to low horizontal (e.g. $10 \times 10\,km^2$

5 for the Moderate Resolution Imaging Spectroradiometers (MODIS), Kaufman et al., 2002) and temporal resolutions (e.g. twice a day for polar orbiting satellites). Passive instruments can only retrieve column-integrated aerosol concentration (Kaufman et al., 2002). Spaceborne lidar promises to improve the vertical resolution of aerosol measurements at the global scale (Winker et al., 2003; Berthier et al., 2006; Chazette et al.,

10 2010). Nevertheless, the spaceborne lidar measurements are only performed following the satellite ground track.

Thanks to the new generation of portable lidar systems developed in the past five years, accurate vertical profiles of aerosols can now be measured (Raut and Chazette, 2007; Chazette et al., 2007). Such instruments document the mid and lower tropo-

15 sphere by means of aerosol optical properties. Lidar measurements were used in several campaigns, such as ESQUIF (Étude et Simulation de la Qualité de l'air en Île-de-France) (Chazette et al., 2005), MEGAPOLI (Megacities: Emissions, urban, regional and Global Atmospheric POLlution and climate effects, and Integrated tools for assessment and mitigation) summer experiment in July 2009 (Royer et al., 2011) and

20 during the eruption of the Icelandic volcano Eyjafjallajökull on 14 April 2010 (Chazette et al., 2012). Raut et Chazette (2009) established a reliable relation between the mass concentration and the optical properties of pollution aerosol. Thereby, the PM_{10} concentrations above urban area can be retrieved from a ground-based lidar system with an uncertainty of about 25 %.

25 Because a lidar network with continuous measurements does not yet exist, lidar observations have not yet been used for DA. This work aims to investigate the usefulness of future ground-based lidar network on analysis and short-term forecasts of PM_{10}. Building and maintaining observing systems with new instruments is very costly, especially for ground-based lidars. Therefore, an Observing System Simulation Experiment

Title Page

Abstract	Introduction
Conclusions	References
Tables	Figures

◀ ▶|

◀ ▶

Back Close

Full Screen / Esc

(OSSE) can be used to effectively test proposed observing strategies before a field experiment takes place, and it can provide valuable information for the design of field experiments (Masutani et al., 2010).

An OSSE system is constituted by a twin run (i.e. an approximate atmosphere), simulated observations, and DA experiments. The twin run is usually a simulation from a high-resolution state-of-the-art model forecast, and is used to create observations and validate DA experiments (Chen et al., 2011). OSSE systems are used for many applications, such as investigating the accuracy of diagnostic heat and moisture budgets (Kuo et al., 1984), studying carbon dioxide measurements from the Orbiting Carbon Observatory using a four-dimensional variational assimilation (Chevallier et al., 2007; Baker et al., 2010), demonstrating the data impact of Doppler wind lidar (Masutani et al., 2010; Tan et al., 2007), defining quantitative trace carbon monoxide measurement requirements for satellite missions (Edwards et al., 2009), comparing the relative capabilities of two geostationary thermal infrared instruments to measure ozone and carbon monoxide (Claeyman et al., 2011), evaluating the contribution of column aerosol optical depth observations from a future imager on a geostationary satellite (Timmermans et al., 2009), studying the impact of observational strategies in field experiments on weather analysis and short-term forecasts (Chen et al., 2011).

This paper is organised as follows. Section 2 provides a description of the DA methodology used in this study. Section 3 describes the experiment setup, i.e. the chemistry transport model used and real observations. An OSSE system is built in Sect. 4. Results of the OSSE are shown in Sects. 5 and 6. Sensitivity studies with respect to the number and locations of lidar stations are conducted in Sect. 7. The findings are summarised and discussed in Sect. 8.

2 Choice of DA method

In an OSSE, DA is performed to couple model with simulated observations. Different DA algorithms may be used, e.g. OI, reduced-rank square root Kalman filter, ensemble

Kalman filter (EnKF) and four-dimensional variational assimilation (4D-Var). Wu et al. (2008) have illustrated their limitations and potentials. They found that in the air quality context the OI provides overall strong performances and it is easy to implement. In the EnKF used in air quality, the model uncertainties are approximated by the statistics of the ensemble generated by perturbing uncertain model parameters. It produces the best forecasts at the end of prediction periods. In terms of performance, the reduced-rank square root Kalman filter is quite similar to EnKF. The strongly constrained 4D-Var provides a moderate performance, because uncertainties are taken into account only at the initial date of the assimilation window. On the other hand, the work of Denby et al. (2008) compared two different DA techniques, the statistical interpolation method and EnKF, for assimilating PM_{10} concentration at the European scale. Denby et al. (2008) showed that statistical interpolation (similar to OI or three-dimensional variational method) can be more effective than the EnKF.

In this paper, we use the OI as it is the simpler method for PM_{10} DA and it performs well (Denby et al., 2008; Wu et al., 2008). Furthermore, the OI method can be used in operational mode for real-time forecast, as the computational cost of OI is low. It was used by Tombette et al. (2009) and Pagowski et al. (2010) for DA of conventional aerosol ground observation. In the OI method, DA is performed at the frequency of measurements to produce analysed concentrations, which are closer to reality (measurements) than forecasts and which are used as initial conditions for the next model iteration. The equations to compute the analysed concentrations from the model concentrations are given in Tombette et al. (2009). They require the specification of the background and observation error covariance matrices (see Sects. 4.2, 4.4 and 5). The background error covariance matrix determines how the corrections of the concentrations should be distributed over the domain during DA. The observation error covariance matrix specifies instrumental and representativeness errors. As in Tombette et al. (2009), after DA of PM_{10} concentrations, the analysed PM_{10} concentrations are redistributed over the model variables following the initial chemical and size distributions.

3 Experimental setup

3.1 Model

For our study, the chemistry transport model Polair3D (Sartelet et al., 2007) of the air-quality platform Polyphemus, available at http://cerea.enpc.fr/polyphemus/ and described in Mallet et al. (2007) is used. Aerosols are modelled using the SIze-REsolved Aerosol Model (SIREAM-SuperSorgam), which is described in Debry et al. (2007) and Kim et al. (2011b). SIREAM-SuperSorgam includes 20 aerosol species: 3 primary species (mineral dust, black carbon and primary organic species), 5 inorganic species (ammonium, sulfate, nitrate, chloride and sodium) and 12 organic species. It models coagulation and condensation. Five bins logarithmically distributed over the size range 0.01–10 µm are used. The gas chemistry is solved with the chemical mechanism CB05 (Carbon Bond version 5) (Yarwood et al., 2005). Polair3D/SIREAM has been used for several applications. For example, it was compared to measurements for gas and aerosols over Europe by Sartelet et al. (2007) and Kim et al. (2010), and it was compared to lidar measurements over Greater Paris by Royer et al. (2011).

3.2 Input data

The modelling domain covers Western and part of Eastern Europe ([10.5° W, 23° E] × [35° N, 58° N]) with a horizontal resolution of 0.5° × 0.5°. Nine vertical levels are considered from the ground to 12 000 m. The heights of the cell interfaces are 0, 40, 120, 300, 800, 1500, 2400, 3500, 6000 and 12 000 m. The simulations are carried out for one month from 15 July to 15 August 2001, with a time step of 600 s. Meteorological inputs are obtained from reanalysis provided by the European Centre for Medium-Range Weather Forecasts (ECMWF). Anthropogenic emissions of gases and aerosols are generated with the EMEP inventory for 2001. For gaseous boundary conditions, daily means are extracted from outputs of the global chemistry-transport model MOZART2 (Model for OZone And Related chemical Tracers version 2) (Horowitz et al.,

2003). For aerosol boundary conditions, daily means are based on outputs of the God-dard Chemistry Aerosol Radiation and Transport model (GOCART) for the year 2001 for sulfate, dust, black carbon and organic carbon (Chin et al., 2000; Sartelet et al., 2007).

3.3 Observational data

In this paper, as in Sartelet et al. (2007) and Tombette et al. (2009), we use the locations of stations of two ground databases for the comparisons to ground data measurements:

- the EMEP database, available on the EMEP Chemical Co-ordinating Centre (EMEP/CCC) website at http://www.emep.int/;

- the AirBase database, available on the European Environment Agency (EEA) website at http://air-climate.eionet.europa.eu/databases/airbase/. Note that the traffic and industrial stations are not used, because the simulation horizontal scale ($0.5° \times 0.5°$) can not be representative of these stations types.

In 2001, PM_{10} concentrations are provided on a daily basis at EMEP stations, against an hourly basis at most AirBase stations. Moreover, data are provided at only 27 EMEP stations, against 509 AirBase stations. Therefore, the EMEP network is only used for the performance assessment of the "true" atmospheric state, whereas the AirBase network is used for the performance assessment of "true" atmospheric state, for as-similations and for evaluating the results of DA experiments in OSSE. Figure 1 shows the location of the EMEP and AirBase stations used in this study.

In this work, a network of 12 ground-based lidar stations is defined, as shown in Fig. 1, using the nine existing locations of the Lidar Environmental Observations NET-work (LEONET, http://leo-net.eu/) and adding 3 fictitious stations in order to cover well Western Europe.

4 Observing system simulation experiment

4.1 Twin run

An important aspect of observation impact experiments of yet non-existing observing systems is the need for an atmospheric state for the simulation of the new observing system. Since the true atmosphere is inherently unknown, a synthetic atmosphere state, in the remainder denoted "truth", needs to be defined. In an OSSE, the "true" state is used to create the observational data from existing and future instruments. In this paper, the "truth" is obtained from a simulation, called twin run, performed between 00:00 UTC 15 July to 00:00 UTC 15 August 2001 using the model (Kim et al., 2010, 2011a) and the input data described in the previous section. Here, we first evaluate the results of this simulation with the AirBase and EMEP networks.

The statistical indicators used to evaluate PM_{10} concentrations are: the Root Mean Square Error (RMSE), the (Pearson) correlation, the Mean Fractional Error (MFE), the Mean Fractional Bias (MFB). Let $\{o_i\}_{i=1,n}$ and $\{s_i\}_{i=1,n}$ be the observed and the modelled concentrations, respectively. Let n be the number of available observations. The statistical indicators are defined as follow:

$$\text{RMSE} = \sqrt{\frac{1}{n}\sum_{i=1}^{n}(o_i - s_i)^2}, \tag{1}$$

$$\text{correlation} = \frac{\sum_{i=1}^{n}(o_i - \bar{o})(s_i - \bar{s})}{\sqrt{\sum_{i=1}^{n}(o_i - \bar{o})^2 \sum_{i=1}^{n}(s_i - \bar{s})^2}}, \tag{2}$$

$$\text{MFE} = \frac{1}{n}\sum_{i=1}^{n}\frac{|s_i - o_i|}{(s_i + o_i)/2}, \tag{3}$$

$$\text{MFB} = \frac{1}{n}\sum_{i=1}^{n}\frac{s_i - o_i}{(s_i + o_i)/2}, \tag{4}$$

where $\bar{o} = \frac{1}{n}\sum_{i=1}^{n} o_i$ and $\bar{s} = \frac{1}{n}\sum_{i=1}^{n} s_i$.

According to Boylan and Russel (2006), if both the MFB (%) and MFE (%) are in [−30%, 30%] and [0, 50%], respectively, then the model performance goal is met; if both the MFB and MFE are in [−60%, 60%] and [0, 75%], respectively, the model performance criterion is met. As shown in Table 1, for PM_{10}, the model performance criterion is met for the two networks, whereas for $PM_{2.5}$ (particulate matter with a diameter smaller than $2.5\,\mu g\,m^{-3}$) both the model performance goal and criterion are met for the two networks, suggesting that this simulation compares well to observations. Furthermore, as shown in Fig. 2, the spatial distribution of PM_{10} concentration corresponds to previously published results (Sartelet et al., 2007). Even though, for an OSSE study, the accuracy of the twin run compared with real observations is usually not a major concern, the twin run should produce typical features of the phenomena of interest. This "true" simulation is subsequently used for the creation of observations from the observing system under investigation and will also be used to evaluate the results of DA experiments (see Sects. 5, 6 and 7).

4.2 Simulated observations and error modelling

After defining the "truth", it is used to calculate the "true" states (e.g. concentrations) of the future ground-based lidar network and the existing network AirBase. For example, Fig. 3 shows the "true" state of PM_{10} at two arbitrary chosen lidar stations: Madrid (Perez et al., 2004) and Saclay (Raut et Chazette, 2009). We find that the high PM_{10} concentrations in Madrid are mostly made of Sahara dust. The "true" state at each station is perturbed depending on estimated observation errors. For the network Air-Base, the observation errors correspond to the representativeness errors, and they are estimated to be about 35 %. For the ground-based lidar network, the observation errors include the representativeness errors (about 35 %) and the instrumental errors, which are estimated to be about 25 % for PM_{10} concentrations obtained from lidar observations (Raut et Chazette, 2009). These instrumental errors are linked to errors in

estimating the extinction coefficients using the inversion of the lidar signal (Klett et al., 1981) and extinction coefficient cross sections. The covariance between the representativeness and instrumental errors is set to zero since they are independent. Finally, the observation errors of the concentrations obtained from the lidar network are estimated to be about 43 % (the square root of the sum of the representativeness error variance and the instrumental error variance, $\sqrt{35\,\%^2 + 25\,\%^2}$).

After defining the observation errors, the observations obtained from the "true" state are perturbed as now explained. For each station, let x be a vector, whose component x_i is a hourly mean concentration and i depends on vertical level and time. The perturbation is implemented as follows:

– Define the observational error covariance matrix $\mathbf{\Sigma}$ by the Balgovind approach (Balgovind et al., 1983). The error covariance between two points is

$$f(d_v, d_t) = e \left(1 + \frac{d_v}{L_v}\right) \exp\left(-\frac{d_v}{L_v}\right) \times \left(1 + \frac{d_t}{L_t}\right) \exp\left(-\frac{d_t}{L_t}\right), \tag{5}$$

where e is the observational error variance, d_v is the vertical distance between the 2 points, d_t is the temporal difference between the 2 points, $L_v = 200\,\text{m}$ and $L_t = 2$ h are the vertical and temporal correlation lengths. Clearly, each component of the covariance matrix depends smoothly on the altitude of the points and time.

– Use the Cholesky decomposition:

$$\mathbf{\Sigma} = \mathbf{CC}^{\mathsf{T}}, \tag{6}$$

where $\mathbf{C}$ is a lower triangular matrix with strictly positive diagonal entries.

The perturbation of x is then

$$x' = x + \mathbf{C}\gamma, \tag{7}$$

where **γ** is a random vector whose components are a standard normal distribution. Figure 4 shows an example of perturbations at an arbitrary chosen station. We can see that the perturbations depend continuously on the vertical level and the time thanks to matrix **C**. The perturbed observations are subsequently used for the assimilation of the ground-based lidar network and AirBase.

4.3 Control run

The control run is a simulation that stands the best modellers' effort to represent the atmosphere with their model. If the same model is used for both the twin run and the control run, this is called an identical twin OSSE; if the twin run model is a different version of the control run model, the OSSEs are called fraternal twin OSSEs (Liu et al., 2007; Masutani et al., 2010). The identical twin OSSEs are easy to set up. Under the identical twin scenario, the numerical model becomes perfect (i.e. no model error); this is counter to what happens in reality (i.e. models are never perfect) and the identical twin OSSEs usually overestimate the impact of observations on model forecasts (Chen et al., 2011). We follow a "perfect model" OSSE setup, in which the model used to generate the "true" observations is the same as the one used in the control run and DA. Input data, such as meteorological fields, emissions (Edwards et al., 2009) or initial conditions (Liu et al., 2007) have therefore to be perturbed. In order to be able to interpret more easily the results, we choose to perturb only initial conditions. This allows us to avoid the complications of defining model errors, and the only source of forecast errors comes from the initial conditions.

Because of the identical twin relationship between the twin and control runs, the impact of PM_{10} DA may be over-optimistic, but it will be so for both ground observations and lidar observations. As in Sect. 4.2, we use the Balvogind approach (Balgovind et al., 1983), the Cholesky decomposition and the normal distribution to perturb all model concentrations (gaseous and aerosols). In air quality models, the impact of initial conditions on PM_{10} concentrations lasts for a few hours to a few days at most. Perturbing both initial gaseous and aerosol of species allow us to increase the duration

of this impact. As shown in Fig. 5, there are higher differences between "true" and perturbed PM_{10} concentrations in certain parts of Europe than others. The principal reason is the normal distribution. It can produce very high or low concentrations in one grid cell. The perturbed initial conditions are not necessarily consistent with the true state of atmosphere, but they are suitable for our experiments with DA.

4.4 Parameters of the DA runs

The experiments consist of two steps: the DA analysis part and the forecast. During the assimilation period, say between $[t_0, t_N]$, at each time step, the observations are assimilated. During the subsequent forecast period, say between $[t_{N+1}, t_T]$, the aerosol concentrations are obtained from the model simulations initialised from the analysed model state at t_N.

Since only the initial conditions are perturbed in our experiments (see Sect. 4.3), the difference between two forecasts initialised with different initial conditions only lasts for a few days. For the choice of t_N, Fig. 6 compares the RMSE between the true observations and the forecast concentrations from 18 July at 01:00 UTC to 20 July at 00:00 UTC, obtained for different assimilation periods varying from 6 h to 3 days and always ending at 00:00 UTC 18 July. The longer the assimilation period is, the lower the RMSE is. An assimilation period of 12 h seems a good compromise between a low RMSE and a short assimilation time.

Two DA runs are performed in our OSSE, depending on whether ground or vertical observations are assimilated. The simulations use the same setup as the one of the control run. We use the perturbed PM_{10} observations that are produced by the twin run (see Sect. 4.2). The first DA run uses only simulated data at AirBase stations. DA is performed from the first level (20 m above the ground) to the sixth level (1950 m above the ground) of the model. The second DA run uses only the ground-based lidar network simulated data. DA is performed from the third level (210 m above the ground; Raut et Chazette, 2009; Royer et al., 2011) to the sixth level (1950 m above the ground).

In this paper, DA experiments are carried out for 27 five-day experiments between 15 July 2001 and 15 August 2001. The first experiment is from 15 to 19 July 2001, the second one is from 16 to 20 July 2001, and so on until 15 August 2001. For each experiment, the observation data are assimilated from 01:00 UTC to 12:00 UTC every
5 hour, thereafter the model runs and produces a forecast for the next four and half days.

In the OI method, the background and observation error covariance matrices need to be set and are crucial for the success of the method. The observation error covariance matrix depends on the observational error variance, which varies with vertical levels. For ground measurements, we set the error variance to be $20\,\mu g^2\,m^{-6}$, the square of
10 35 % (see Sect. 4.2) of PM_{10} concentration averaged over AirBase stations. For lidar measurement, we set the error variance to be the square of 43 % ($\sqrt{35\%^2 + 25\%^2}$, see Sect. 4.2) of PM_{10} concentration averaged over lidar stations for each level from the third level to the sixth level, which is respectively 28, 24, 16 and $5\,\mu g^2\,m^{-6}$.

In the Balgovind parametrisation of the background error covariance matrix (Wu
15 et al., 2008; Tombette et al., 2009), the variance v is set to $60\,\mu g^2\,m^{-6}$, which is obtained from the difference between the twin run and the control run. The correct specification of the background error correlations is crucial to the quality of the analysis, because they determine to what extent the background fields will be corrected to match the observations. The horizontal correlation length and the vertical correlation length are
20 two parameters of the Balgovind approach. The next section details the choice of the horizontal and vertical correlation length.

5 Choice of the horizontal and vertical correlation lengths

While the definition of background error correlations are relatively trivial, since they correspond to the difference between the background state and the true state, the
25 true atmospheric state is never exactly known. For the choice of the horizontal correlation length L_h and the vertical correlation length L_v, the National Meteorological Center (NMC) method (Parrish and Derber, 1992) is thus used. The background error

is estimated by the differences of PM_{10} concentrations between two simulations. The two simulations start with the same initial conditions and last 24 h. A 24 h forecast is performed in the first simulation, while AirBase data of PM_{10} concentrations are assimilated hourly in the second simulation. In the analysis, the background error covariance matrix is assumed to be a diagonal matrix to avoid making an issue of special error correlations used in the NMC method. In order to eliminate potential bias due to the diurnal cycle, 24 h forecasts are issued at 00:00 UTC and 12:00 UTC. This estimation of the background error is performed for 27 consecutive days from 15 July 2001 at 00:00 UTC and 12:00 UTC.

To estimate the horizontal correlation length, at each model level, we calculate the covariance value for each grid point pair. We then obtain a cloud of covariance values. The covariance clouds are averaged within continuous tolerance regions. The length of the tolerance region is set to 4 grid units, so that there are enough grid point pairs for each tolerance region. Thus, L_h is estimated at all model levels by a least-square fitting of Balgovind functions to the curves of the regionalized covariances. Figure 7 shows the horizontal correlation length L_h of the background error covariance matrix at 00:00 UTC and 12:00 UTC. The variation of the horizontal correlation length is comparable to meteorology (Daley, 1991). The horizontal correlation length is relatively constant in the boundary layer, and it is about 4 grid units (200 km). Above the boundary layer, the horizontal correlation length decreases rapidly. In the DA experiments, we should therefore use a horizontal correlation length scale of 200 km. Similarly to the horizontal correlation length, we find that the vertical correlation length L_v is about 250 m at the ground level.

Although the NMC method gives us estimates of the horizontal and vertical correlation lengths, DA tests with different correlation lengths are performed to assess the optimum lengths, i.e. the lengths which lead to the best forecast. The different tests performed are summarised in Table 2. Assimilation is performed with three different horizontal lengths: $L_h = 50$ km, $L_h = 200$ km and $L_h = 400$ km. For AirBase DA, assimilation is also performed with three different vertical correlation lengths: $L_v = 250$ m,

$L_v = 1500\,\text{m}$ and L_v varying between nighttime and daytime. Because lidar can give us aerosol vertical profiles, we do not consider L_v in the background error covariance matrix (we assume $L_v = 0$). Moreover, column DA tests with different L_v show that $L_v \neq 0$ does not lead to a better forecast for the column DA run. The scores (RMSE and correlation) calculated over land grid points from the ground level to the sixth level (1950 m above the ground) are shown in Fig. 8. For AirBase DA, choosing $L_v = 1500\,\text{m}$ (DA test 3) leads to better scores (lower RMSE and lower correlation) than choosing $L_v = 250\,\text{m}$ (DA test 2), as estimated from the NMC method. Choosing $L_v = 50\,\text{m}$ in the nighttime and $L_v = 1500\,\text{m}$ in the daytime (DA test 4) does not lead to better scores than $L_v = 1500\,\text{m}$ (DA test 3). A possible explanation is that the particles are mixed by turbulence more effectively in the model than in the true state of the atmosphere. The comparison of DA tests 1, 3 and 5 for AirBase and DA tests 6, 7 and 8 for the lidar network shows that $L_h = 200\,\text{km}$, as estimated from the NMC method, leads to good scores. The scores are better than with $L_h = 50\,\text{km}$, and similar to those obtained with $L_h = 400\,\text{km}$.

We also studied the sensitivity of the results to the maximum altitude at which PM_{10} DA is performed during the column DA. We tested the column DA until the eighth level (4750 m above the ground) instead of the sixth level (1950 m above the ground). We found a limited difference in the PM_{10} forecast at the ground level. It is mostly because the planetary boundary layer (PBL) is usually less than 2000 m, and PM_{10} concentrations above the PBL have limited impacts on surface PM_{10}. PM_{10} concentrations at higher levels are low (Royer et al., 2011).

6 Comparison between AirBase and 12 lidars network DA

In the following, we compare the DA test 3 for AirBase ($L_h = 200\,\text{km}$ and $L_v = 1500\,\text{m}$) and the DA test 7 of Fig. 8 for lidar network ($L_h = 200\,\text{km}$ and $L_v = 0$).

Globally, the simulations with DA lead to better scores (lower RMSE and higher correlations) than the simulation without DA. But as shown in Tombette et al. (2009), the

Data assimilation

Y. Wang et al.

Title Page

Abstract | Introduction

Conclusions | References

Tables | Figures

◄ | ►

◄ | ►

Back | Close

Full Screen / Esc

Discussion Paper | Discussion Paper | Discussion Paper | Discussion Paper

assimilation procedure has almost no impact on PM_{10} concentrations after several days of forecast, because assimilation influences only initial conditions and the influence of initial conditions on PM_{10} concentrations does not last for more than a few days. The AirBase DA forecast has always better scores than the column DA forecast in the first

5 several hours of assimilation (to the left of the black line). This may be explained by the fact that the AirBase DA run assimilates from the first level of the model (20 m above the ground) to the sixth level (1950 m above the ground) and the column DA run assimilates from the third level (210 m above the ground) to the sixth level (1950 m above the ground). It takes several hours for the column DA to influence ground concentrations.

10 However, during the forecast period, the RMSE of the column DA run decreases faster than the AirBase DA run (to the right of the black line). After 24 h forecast, the column DA has better scores than the AirBase DA run. It is mostly because the impact of the column DA run is higher than the AirBase DA run's at high levels.

Figure 9 shows the RMSE for the PM_{10} forecast without DA, with the AirBase DA

15 and with the column DA for each one-day forecast period between 15 July and 10 August. Assimilation improves the forecast RMSE for each forecast. The averaged RMSE over all forecasts is 9.1 μg m^{-3} without DA, 3.7 μg m^{-3} (decreased about 59 %) with the AirBase DA and 4.2 μg m^{-3} (decreased about 54 %) with the column DA. Although the AirBase DA leads to lower RMSE than the column DA for most forecasts, the column

20 DA can also lead to lower or similar RMSE as the AirBase DA for some forecasts, e.g. the forecasts starting 19, 20, 21, 23, 26 July and 3, 5, 8 August. It is mostly because the lidar network provides more accurate informations than AirBase on those days at high altitude, e.g. Sahara dust in Madrid as shown in Fig. 3 (upper panel). Figure 10 shows the RMSE for the PM_{10} forecast without DA, with the AirBase DA and with the

25 column DA during the second forecast day for each experiment between 15 July and 10 August. The averaged RMSE over all forecasts is 6.1 μg m^{-3} without DA, 2.7 μg m^{-3} (decreased about 56 %) with the AirBase DA and 2.6 μg m^{-3} (decreased about 57 %) with the column DA. Moreover, the column DA leads to lower or similar RMSE as the AirBase DA for most forecasts. The results show a potentially powerful impact of lidar

networks (12 stations) compared to ground networks (488 stations) to improve PM_{10} forecast. We will study the sensitivity to the number and to the lidars locations in the next section.

7   Sensitivity to the number and position of lidars

In this section, we study the sensitivity of the results to the number and to the locations of lidars. Forecasts after DA with four different lidar networks are compared to DA with the previously-used lidar network (blue discs in Fig. 11). DA is performed with another lidar network of 12 lidar stations (denoted Network 1, yellow discs in Fig. 11), with a lidar network of 26 stations (denoted Network 2, magenta diamonds in Fig. 11), with a lidar network of 76 stations (denoted Network 3, cyan thin diamonds in Fig. 11) and DA with a lidar network made of all AirBase stations over Western Europe (denoted Network 4, the red triangles in Fig. 1).

Figures 12 and 13 show the time evolution of the RMSE and the correlation respectively, averaged over all land grids and the vertical for the different tests. Comparing the previously-used lidar network with Network 1 in Fig. 11, we can see that although they have the same number of stations, the locations are very different. Network 1 stations are better spread out over Europe than the previously-used lidar network. Network 1 leads to better scores in the first forecast day than the reference network. This shows that the lidar stations need to be regularly distributed over Europe to globally improve the PM_{10} forecast. The lidar networks 2, 3 and 4 which have more lidar stations perform better (lower RMSE, higher correlation) than the two others. The lidar network 2 DA run has less than $0.15\,\mu g\,m^{-3}$ of RMSE higher than AirBase DA at the beginning of forecast window and has better score than AirBase DA run after several hours forecast. If one increases the number of lidar stations from 26 to 76, the lidar network 3 DA run has better scores than AirBase DA run at the beginning of forecast window and has better scores than AirBase DA during the forecast days. One introduces the lidar network 4 to show that increasing the number of lidars from 76 to about 500 can always improve the

Full Screen / Esc

Printer-friendly Version

Interactive Discussion

forecast scores. Although increasing the number of lidar gives better forecast scores, such lidar networks may be too expensive.

8 Conclusions

In order to investigate the potential impact of a ground-based lidar network on short-term forecasts of PM_{10}, an OSSE has been implemented. We have compared the impacts of assimilating ground-based lidar network data to assimilating the AirBase surface network data. The results shown in this paper suggest that the assimilation of lidar observation would improve PM_{10} forecast over Europe. Because we made several simplifying assumptions: we used an identical twin scenario (perfect model) and assumed uncorrelated observational errors, the PM_{10} improvements from assimilating lidar and ground observations may be over optimistic. The RMSE between one-day forecast and the truth states is improved on average over the summer month from 15 July to 15 August 2001 by 54 % by the lidar DA if 12 lidars are used, against 59 % by the AirBase DA. During the second forecast day, the RMSE is improved on average over the summer month from 15 July to 15 August 2001 by 57 % by the lidar DA, against 56 % by the AirBase DA.

A sensitivity analysis has also been conducted on the number and locations of lidars. We found that spreading out the lidars regularly over Europe can improve the PM_{10} forecast. The RMSE between one-day forecast and the truth states is improved on average over the summer month from 15 July to 15 August 2001 by 57 % by the lidar DA if 12 lidars optimised are used, against 59 % by the AirBase DA. Although increasing the number of lidar improves the forecast scores, a lidar network with many stations may be too expensive.

The main purpose of this work was to demonstrate the potential impact of a ground-based lidar network on short-term forecasts of PM_{10}. Because we did not have enough available lidar observations in Western Europe, we did not perform DA with a combination of real lidar and AirBase observations. A relation between mass concentration and

Data assimilation

Y. Wang et al.

Back | Close

Full Screen / Esc

Printer-friendly Version

Interactive Discussion

optical properties of aerosols was used. Such relation has been determined for pollution aerosols over Greater Paris. However, it needs to be generalised to other measurement sites. For future works, we will use real measurements from lidar stations, directly assimilating the lidar signals in the chemistry transport model and performing DA with a combination of lidar and AirBase observations.

References

Baker, D. F., Bösch, H., Doney, S. C., O'Brien, D., and Schimel, D. S.: Carbon source/sink information provided by column CO_2 measurements from the Orbiting Carbon Observatory, Atmos. Chem. Phys., 10, 4145–4165, doi:10.5194/acp-10-4145-2010, 2010. 23295

Balgovind, R., Dalcher, A., Ghil, M., and Kalnay, E.: A stochastic- dynamic model for the spatial structure of forecast error statistics, Mon. Weather Rev., 111, 701–722, 1983. 23301, 23302

Barker, J. and Tingey, D. T.: Air Pollution Effects on Biodiversity, Springer, New York, 304 pp., 1992. 23293

Berthier, S., Chazette, P., Couvert, P., Pelon, J., Dulac, F., Thieuleux, F., Moulin, C., and Pain, T.: Desert dust aerosol columnar properties over ocean and continental Africa from Lidar in-Space Technology Experiment (LITE) and Meteosat synergy, J. Geophys. Res., 111, D21202, doi:10.1029/2005JD006999, 2006. 23294

Bouttier, F. and Courtier, P.: Data assimilation concepts and methods, Meteorological Training Course Lecture Series, ECMWF, 2001. 23293

Boylan, J. W. and Russell, A. G.: PM and light extinction model performance metrics, goals, and criteria for three-dimensional air quality models, Atmos. Environ., 40, 4946–4959, 2006. 23300

Brandt, J., Christensen, J. H., Frohn, L. M., Geels, C., Hansen, K. M., Hedegaard, G. B., Hvidberg, M., and Skjøth, C. A.: THOR – an operational and integrated model system for air pollution forecasting and management from regional to local scale, Proceedings of the 2nd ACCENT Symposium, Urbino (Italy), July 23–27, 2007. 23293

Chazette, P., Randriamiarisoa, H., Sanak, J., and Couvert P.: Optical properties of urban aerosol from airborne and ground-based in situ measurements performed during the ESQUIF program, J. Geophys. Res, 110, D02206, doi:10.1029/2004JD004810, 2005. 23294

Chazette, P., Sanak, J., and Dulac, F.: New approach for aerosol profiling with a lidar onboard an ultralight aircraft: application to the African monsoon multidisciplinary analysis, Environ. Sci. Technol., 41, 8335–8341, 2007. 23294

Chazette, P., Raut, J.-C., Dulac, F., Berthier, S., Kim, S.-W., Royer, P., Sanak, J., Loaëc, S., and Grigaut-Desbrosses, H.: Simultaneous observations of lower tropospheric continental aerosols with a ground-based, an airborne, and the spaceborne CALIOP lidar systems, J. Geophys. Res., 115, D00H31, doi:/10.1029/2009JD012341, 2010. 23294

Chazette, P., Bocquet, M., Royer, P., Winiarek, V., Raut, J.-C., Labazuy, P., Gouhier, M., Lardier, M., and Cariou, J.-P.: Eyjafjallajökull ash concentrations derived from both Lidar and modeling, J. Geophys. Res.-Atmos., 117, D00U14, doi:10.1029/2011JD015755, 2012. 23294

Chen, S.-H., Chen, J.-Y., Chang, W.-Y., Lin, P.-L., Lin, P.-H. and Sun, W.-Y.: Observing system simulation experiment: development of the system and preliminary results, J. Geophys. Res., 116, D13202, doi:10.1029/2010JD015103, 2011. 23295, 23302

Chevallier, F., Bréon, F.-M., and Rayner, P. J.: Contribution of the orbiting carbon observatory to the estimation of CO_2 sources and sinks: theoretical study in a variational data assimilation framework, J. Geophys. Res., 112, D09307, doi:10.1029/2006JD007375, 2007. 23295

Chin, M., Rood, R. B., Lin, S.-J., Müller, J.-F., and Thompson, A. M.: Atmospheric sulfur cycle simulated in the global model GOCART: model description and global properties, J. Geophys. Res., 105, 24671–24687, 2000. 23298

Claeyman, M., Attié, J.-L., Peuch, V.-H., El Amraoui, L., Lahoz, W. A., Josse, B., Joly, M., Barré, J., Ricaud, P., Massart, S., Piacentini, A., von Clarmann, T., Höpfner, M., Orphal, J., Flaud, J.-M., and Edwards, D. P.: A thermal infrared instrument onboard a geostationary

platform for CO and O_3 measurements in the lowermost troposphere: Observing System Simulation Experiments (OSSE), Atmos. Meas. Tech., 4, 1637–1661, doi:10.5194/amt-4-1637-2011, 2011. 23295

Daley, R.: Atmospheric Data Analysis, Cambridge University Press, 1991. 23305

5 De Wildt, M. D., Eskes, H., Manders, A., Sauter, F., Schaap, M., Swart, D., and van Velthoven, P.: Six-day PM_{10} air quality forecasts for the Netherlands with the chemistry transport model Lotos-Euros, Atmos. Environ., 45, 5586–5594, doi:10.1016/j.atmosenv.2011.04.049, 2011.

Debry, E., Fahey, K., Sartelet, K., Sportisse, B., and Tombette, M.: Technical Note: A new SIze REsolved Aerosol Model (SIREAM), Atmos. Chem. Phys., 7, 1537–1547, doi:10.5194/acp-7-1537-2007, 2007. 23297

10 Denby, B., Schaap, M., Segers, A., Builtjes, P., and Horálek, J.: Comparison of two data assimilation methods for assessing PM_{10} exceedances on the European scale, Atmos. Environ., 42, 7122–7134, 2008. 23293, 23296

Dickerson, R. R., Kondragunta, S., Stenchikov, G., Civerolo, K. L., Doddrige, B. G., and Holben, B. N.: The impact of aerosols on solar ultraviolet radiation and photochemical smog, Science, 278, 827–830, 1997. 23293

Dockery, D. and Pope, A.: Epidemiology of acute health effects: summary of time-series, in: Particles in our Air: Concentration and Health Effects, edited by: Wilson, R. and Spengler, J. D., Harvard University Press, Cambridge, MA, USA, 123–147, 1996. 23293

20 Edwards, D. P., Arellano Jr., A. F., and Deeter, M. N.: A satellite observation system simulation experiment for carbon monoxide in the lowermost troposphere, J. Geophys. Res., 114, D14304, doi:10.1029/2008JD011375, 2009. 23295, 23302

Elbern, H., Schwinger, J., and Botchorishvili, R.: Chemical state estimation for the middle atmosphere by four-dimensional variational data assimilation: system configuration, J. Geophys. Res.-Atmos., 115, D06302, doi:10.1029/2009JD011953, 2010.

25 Hodzic, A., Vautard, R., Chazette, P., Menut, L., and Bessagnet, B.: Aerosol chemical and optical properties over the Paris area within ESQUIF project, Atmos. Chem. Phys., 6, 3257–3280, doi:10.5194/acp-6-3257-2006, 2006. 23293

Horowitz, L., Walters, S., Mauzerall, D., Emmons, L., Rasch, P., Granier, C., Tie, X., Lamarque, J.-F., Schultz, M., Tyndall, G., Orlando, J., and Brasseur, G.: A global simulation of tropospheric ozone and related tracers: description and evaluation of MOZART, version 2, J. Geophys. Res., 108, 4784, doi:10.1029/2002JD002853, 2003. 23297

Title Page

Abstract | Introduction

Conclusions | References

Tables | Figures

◄ | ►|

◄ | ►

Back | Close

Full Screen / Esc

Printer-friendly Version

Interactive Discussion

Intergovernment Panel on Climate Control (IPCC): Climate Change 2007, the Fourth Assessment Report of the IPCC, Cambridge Univ. Press, New York, 2007. 23293

Kalnay, E.: Atmospheric Modeling, Data Assimilation, and Predictability, Cambridge University Press, Cambridge, United Kingdom, 341 pp., 2003. 23293

5 Kaufman, Y. J., Tanré, D., and Boucher, O.: A satellite view of aerosols in the climate system, Nature, 419, 215–223, 2002. 23294

Kim, Y., Sartelet, K. N., and Seigneur, C.: Comparison of two gas-phase chemical kinetic mechanisms of ozone formation over Europe, J. Atmos. Chem., 62, 89–119, 2010. 23297, 23299

Kim, Y., Sartelet, K., and Seigneur, C.: Formation of secondary aerosols over Europe: comparison of two gas-phase chemical mechanisms, Atmos. Chem. Phys., 11, 583–598, doi:10.5194/acp-11-583-2011, 2011a. 23299

Kim, Y., Couvidat, F., Sartelet, K., and Seigneur, C.: Comparison of different gas-phase mechanisms and aerosol modules for simulating particulate matter formation, J. Air Waste Manag. Assoc., 61, 1218–1226, doi:10.1080/10473289.2011.603999, 2011b. 23297

15 Klett, J. D.: Stable analytical inversion solution for processing lidar returns, Appl. Optics, 20, 211–220, 1981. 23301

Konovalov, I. B., Beekmann, M., Meleux, F., Dutot, A., and Foret, G.: Combining deterministic and statistical approaches for PM(10) forecasting in Europe, Atmos. Environ., 43, 6425–6434, doi:10.1016/j.atmosenv.2009.06.039, 2009.

20 Kuo, Y.-H. and Anthes, R. A.: Accuracy of diagnostic heat and moisture budgets using SESAME-79 field data as revealed by observing system simulation experiments, Mon. Weather Rev., 112, 1465–1481, 1984. 23295

Lahoz, W., Khattatov, B., and Ménard, R. (Eds.): Data Assimilation Making Sense of Observations, Springer, Berlin, Germany, 718 pp., 2010. 23293

25 Lauwerys, R. R.: Toxicologie industrielle et intoxications professionnelles, Masson, 1982. 23293

Léon, J. F., Chazette, P., Pelon, J., Dulac, F., and Ramdriamarisoa H.: Aerosol direct radiative impact over the INDOEX area based on passive and active remote sensing, J. Geophys. Res., 107, D198006, doi:10.1029/2000JD000116, 2002. 23293

Liu, J. and Kalnay, E.: Simple Doppler wind lidar adaptive observation experiments with 3D-Var 30 and an ensemble Kalman filter in a global primitive equations model, Geophys. Res. Lett., 34, L19808, doi:10.1029/2007GL030707, 2007. 23302

Mallet, V., Quélo, D., Sportisse, B., Ahmed de Biasi, M., Debry, É., Korsakissok, I., Wu, L., Roustan, Y., Sartelet, K., Tombette, M., and Foudhil, H.: Technical Note: The air quality

Data assimilation

Y. Wang et al.

Title Page

Abstract	Introduction
Conclusions	References
Tables	Figures

|◄ | ►|

◄ | ►

Back | Close

Full Screen / Esc

Printer-friendly Version

Interactive Discussion

modeling system Polyphemus, Atmos. Chem. Phys., 7, 5479–5487, doi:10.5194/acp-7-5479-2007, 2007. 23297

Masutani, M., Woollen, J. S., Lord, S. J., Emmitt, G. D., Kleespies, T. J., Wood, S. A., Greco, S., Sun, H., Terry, J., Kapoor, V., Treadon, R., and Campana, K. A.: Observing system simulation experiments at the National Centers for Environmental Prediction, J. Geophys. Res., 115, D07101, doi:10.1029/2009JD012528, 2010. 23295, 23302

Niu, T., Gong, S. L., Zhu, G. F., Liu, H. L., Hu, X. Q., Zhou, C. H., and Wang, Y. Q.: Data assimilation of dust aerosol observations for the CUACE/dust forecasting system, Atmos. Chem. Phys., 8, 3473–3482, doi:10.5194/acp-8-3473-2008, 2008. 23293

Pagowski, M., Grell, G. A., McKeen, S. A., Peckham, S. E., and Devenyi, D.: Three-dimensional variational data assimilation of ozone and fine particulate matter observations: some results using the Weather Research and Forecasting–Chemistry model and grid-point statistical interpolation, Q. J. Roy. Meteorol. Soc., 136, 2013–2024, doi:10.1002/qj.700, 2010. 23293, 23296

Parrish, D. F. and Derber, J. C.: The National Meteorological Center's spectral statistical interpolation analysis system, Mon. Weather Rev., 120, 1747–1763, 1992. 23304

Perez, C., Sicard, M., Jorba, O., Comeron, A., and Baldasano, J. M.: Summertime recirculations of air pollutants over the North-Eastern Iberian coast observed from systematic EARLINET lidar measurements in Barcelona, Atmos. Environ., 38, 3983–4000, 2004. 23300

Randriamiarisoa, H., Chazette, P., and Mégie, G.: The columnar retrieved single scattering albedo from NO_2 photolysis rate, Tellus B, 56, 118–127, 2004. 23293

Ramanathan, V., Crutzen, P. J., Lelieveld, J., Mitra, A. P., Althausen, D., Anderson, J., Andreae, M. O., Cantrell, W., Cass, G. R., Chung, C. E., Clarke, A. D., Coakley, J. A., Collins, W. D., Conant, W. C., Dulac, F., Heintzenberg, J., Heymsfield, A. J., Holben, B., Howell, S., Hudson, J., Jayaraman, A., Kiehl, J. T., Krishnamurti, T. N., Lubin, D., McFarquhar, G., Novakov, T., Ogren, J. A., Podgorny, I. A., Prather, K., Priestley, K., Prospero, J. M., Quinn, P. K., Rajeev, K., Rasch, P., Rupert, S., Sadourny, R., Satheesh, S. K., Shaw, G. E., Sheridan, P., and Valero, F. P. J.: The Indian Ocean Experiment: an integrated assessment of the climate forcing and effects of the great Indo-Asian haze, J. Geophys. Res., 106, 28371–28398, 2001. 23293

Roustan, Y., Sartelet, K. N., Tombette, M., Debry, É, and Sportisse, B.: Simulation of aerosols and gas-phase species over Europe with the POLYPHEMUS system, Part II: Model sensitivity analysis for 2001, Atmos. Environ., 44, 4219–4229, 2010. 23293

Data assimilation

Y. Wang et al.

Title Page

Abstract	Introduction
Conclusions	References
Tables	Figures

◄ | ►|

◄ | ►

Back | Close

Full Screen / Esc

Printer-friendly Version

Interactive Discussion

Raut, J.-C. and Chazette, P.: Retrieval of aerosol complex refractive index from a synergy between lidar, sunphotometer and in situ measurements during LISAIR experiment, Atmos. Chem. Phys., 7, 2797–2815, doi:10.5194/acp-7-2797-2007, 2007. 23294

Raut, J.-C. and Chazette, P.: Assessment of vertically-resolved PM_{10} from mobile lidar observations, Atmos. Chem. Phys., 9, 8617–8638, doi:10.5194/acp-9-8617-2009, 2009. 23294, 23300, 23303

Royer, P., Chazette, P., Sartelet, K., Zhang, Q. J., Beekmann, M., and Raut, J.-C.: Lidar-derived PM_{10} and comparison with regional modeling in the frame of the MEGAPOLI Paris summer campaign, Atmos. Chem. Phys. Discuss., 11, 11861–11909, doi:10.5194/acpd-11-11861-2011, 2011. 23294, 23297, 23303, 23306

Sartelet, K. N., Debry, E., Fahey, K. M., Roustan, Y., Tombette, M., and Sportisse, B.: Simulation of aerosols and gas-phase species over Europe with the Polyphemus system, Part I: Model-to-data comparison for 2001, Atmos. Environ., 29, 6116–6131, 2007. 23293, 23297, 23298, 23300

Schaap, M., Spindler, G., Schulz, M., Acker, K., Maenhaut, W., Berner, A., Wieprecht, W., Streit, N., Müller, K., Brüggemann, E., Chi, X., Putaud, J.-P., Hitzenberger, R., Puxbaum, H., Baltensperger, U., and ten Brink, H.: Artefacts in the sampling of nitrate studied in the "INTERCOMP" campaigns of EUROTRAC-AEROSOL, Atmos. Environ., 48, 6487–6496, 2004. 23293

Sheridan, P. J., Jefferson, A., and Ogren, J. A.: Spatial variability of submicrometer aerosol radiative properties over the Indian Ocean during INDOEX, J. Geophys. Res., 107, D198011, doi:10.1029/2000JD000166, 2002. 23293

Simpson, D., Fagerli, H., Jonson, J. E., Tsyro, S., Wind, P., and Tuovinen, J.-P.: Transboundary acidification, euthrophication and ground level ozone in Europe, Part I: Unified EMEP model description, Technical Report, EMEP, 2003. 23293

Tan, D. G. H., Andersson, E., Fisher, M., and Isaksen, L.: Observing system impact assessment using a data assimilation ensemble technique: application to the ADM-Aeolus wind profiling mission, Q. J. Roy. Meteorol. Soc., 133, 381–390, 2007. 23295

Timmermans, R. M. A., Segers, A. J., Builtjes, P. J. H., Vautard, R., Siddans, R., Elbern, H., Tjemkes, S. A. T., and Schaap, M.: The added value of a proposed satellite imager for ground level particulate matter analyses and forecasts, IEEE J. Sel. Topics Appl. Earth Obs. Remote Sens., 2, 271–283, 2009. 23295

Title Page

Abstract | Introduction

Conclusions | References

Tables | Figures

◄ | ►

◄ | ►

Back | Close

Full Screen / Esc

Printer-friendly Version

Interactive Discussion

Tombette, M., Mallet, V., and Sportisse, B.: PM_{10} data assimilation over Europe with the optimal interpolation method, Atmos. Chem. Phys., 9, 57–70, doi:10.5194/acp-9-57-2009, 2009. 23293, 23296, 23298, 23304, 23306

Winker, D. M., Pelon, J., and McCormick, M. P.: The CALIPSO mission: spaceborne lidar for observation of aerosols and clouds, Proc. SPIE, 4893, 1, doi:10.1117/12.466539, 2003. 23294

Wu, L., Mallet, V., Bocquet, M., and Sportisse, B.: A comparison study of data assimilation algorithms for ozone forecasts, J. Geophys. Res., 113, D20310, doi:10.1029/2008JD009991, 2008. 23296, 23304

Yarwood, G., Rao, S., Yocke, M., and Whitten, G.: Updates to the Carbon Bond Chemical Mechanism: CB05 Final Report to the US EPA, RT-0400675, available at: http://www.camx.com/camx/files/a2/a276b632-c133-46fd-aba0-cf2c0d2e4a30.pdf, 2005. 23297

Table 1. Statistics of the simulation results for the AirBase and EMEP networks from 15 July to 14 August. Ammon. stands for ammonium. Obs. stands for observation. Sim. stands for simulation. Corr. stands for correlation.

Species	Database	Stations	Obs. mean $\mu g\,m^{-3}$	Sim. mean $\mu g\,m^{-3}$	RMSE $\mu g\,m^{-3}$	Corr. %	MFB %	MFE %
PM_{10}	AirBase	419	22.5	12.7	17.3	35	−47	69
	EMEP	27	18.8	12.3	9.6	67	−39	48
$PM_{2.5}$	AirBase	3	11.2	13.1	8.7	45	7	44
	EMEP	18	13.2	11.5	7.2	64	−16	45
Sulfate	AirBase	11	2.2	3.0	1.7	59	41	60
	EMEP	51	2.9	2.6	1.7	61	−3	45
Nitrate	AirBase	8	2.8	5.1	4.0	51	23	72
	EMEP	13	1.7	2.2	1.9	20	−16	78
Ammon.	AirBase	8	1.7	2.5	1.3	62	28	43
	EMEP	8	1.6	1.8	1.1	39	6	47
Sodium	EMEP	1	1.4	2.4	1.6	82	44	52
Chloride	AirBase	7	0.6	2.2	1.9	70	1	1

Title Page

Abstract | Introduction

Conclusions | References

Tables | Figures

◀◀ | ▶▶

◀ | ▶

Back | Close

Full Screen / Esc

Printer-friendly Version

Interactive Discussion

Table 2. DA tests with different configurations for Balgovind Scale Parameters.

Simulation name	AirBase DA	Column DA	L_h (km)	L_v (m)
DA test 1	×		50	1500
DA test 2	×		200	250
DA test 3	×		200	1500
DA test 4	×		200	50 (nighttime)
				1500 (daytime)
DA test 5	×		400	1500
DA test 6		×	50	0
DA test 7		×	200	0
DA test 8		×	400	0
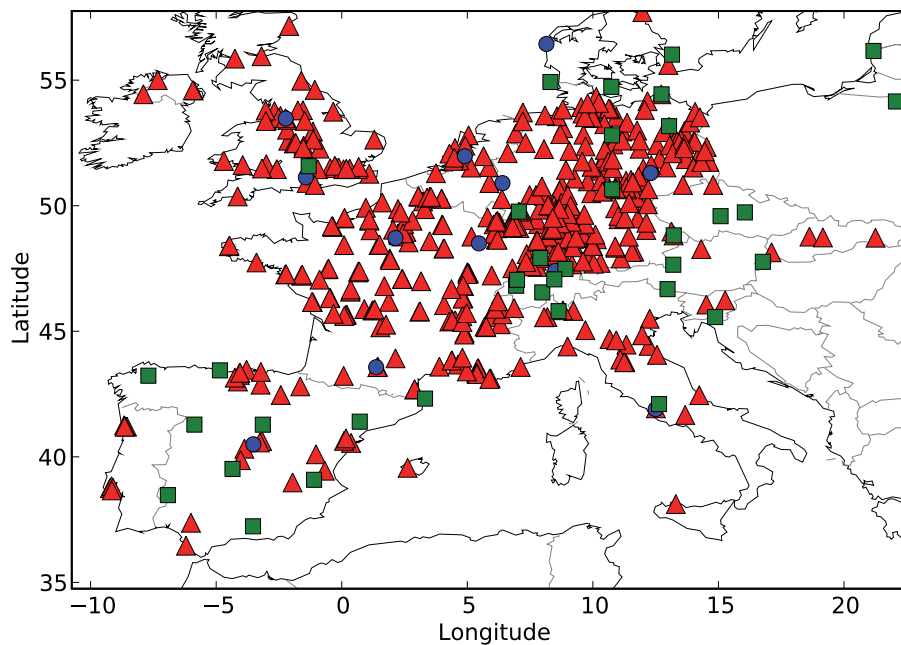
Fig. 1. The green squares show the locations of EMEP stations, the red triangles show the locations of AirBase stations, and the blue discs show the locations of the lidar network.
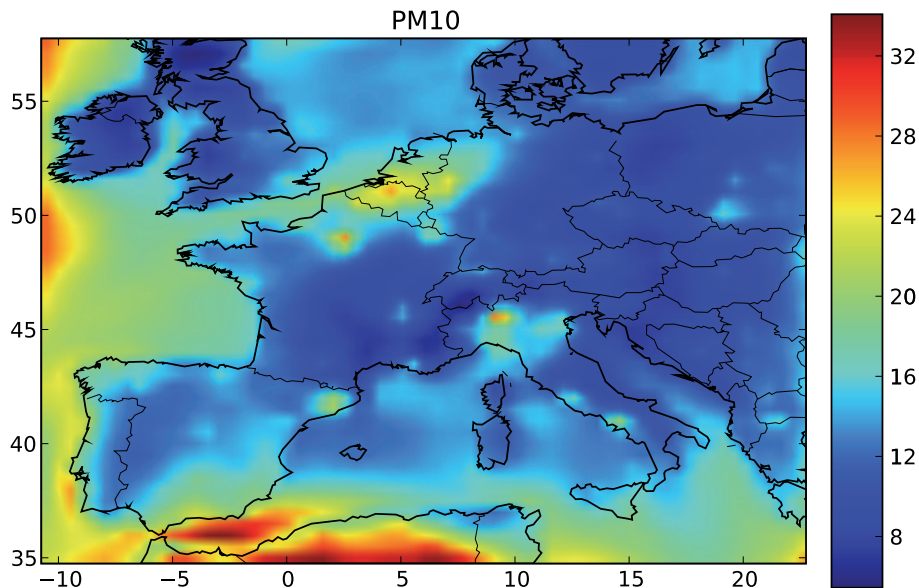
Fig. 2. Mean concentrations of PM_{10} over Europe (in $\mu g\,m^{-3}$). It ranges from $6\,\mu g\,m^{-3}$ (dark blue) to $34\,\mu g\,m^{-3}$ (dark red).

Full Screen / Esc

Printer-friendly Version

Interactive Discussion
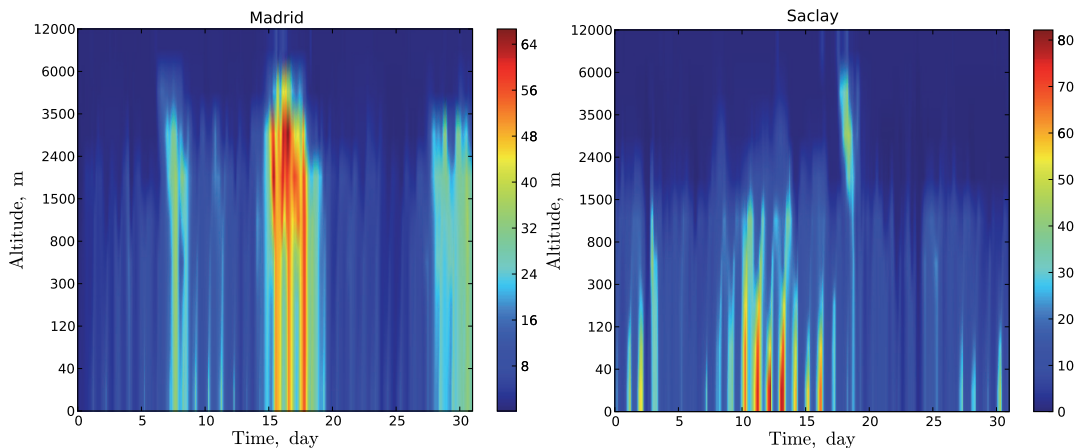
Fig. 3. The "true" state of PM_{10} from 01:00 UTC 15 July to 00:00 UTC 15 August 2001 at the lidar stations Madrid (upper panel) and Saclay (lower panel). Dark and red colours correspond to high and low PM_{10} concentrations, respectively.

Title Page

Abstract   Introduction

Conclusions   References

Tables   Figures

◄◄   ►►

◄   ►

Back   Close

Full Screen / Esc

Printer-friendly Version

Interactive Discussion
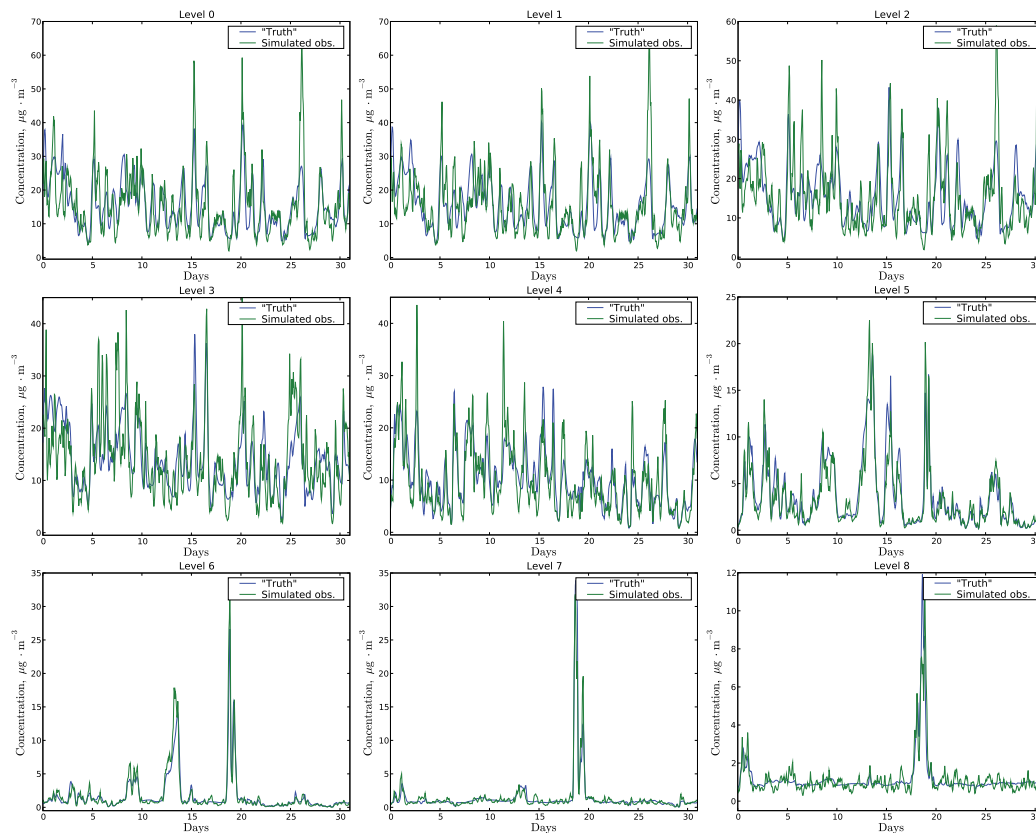
Fig. 4. Perturbation at a random AirBase station from 15 July to 15 August 2001 at from first to last vertical level of the model. The blue lines show the "true" PM_{10} concentrations ($\mu g\,m^{-3}$). The green lines show the simulated PM_{10} concentrations ($\mu g\,m^{-3}$).
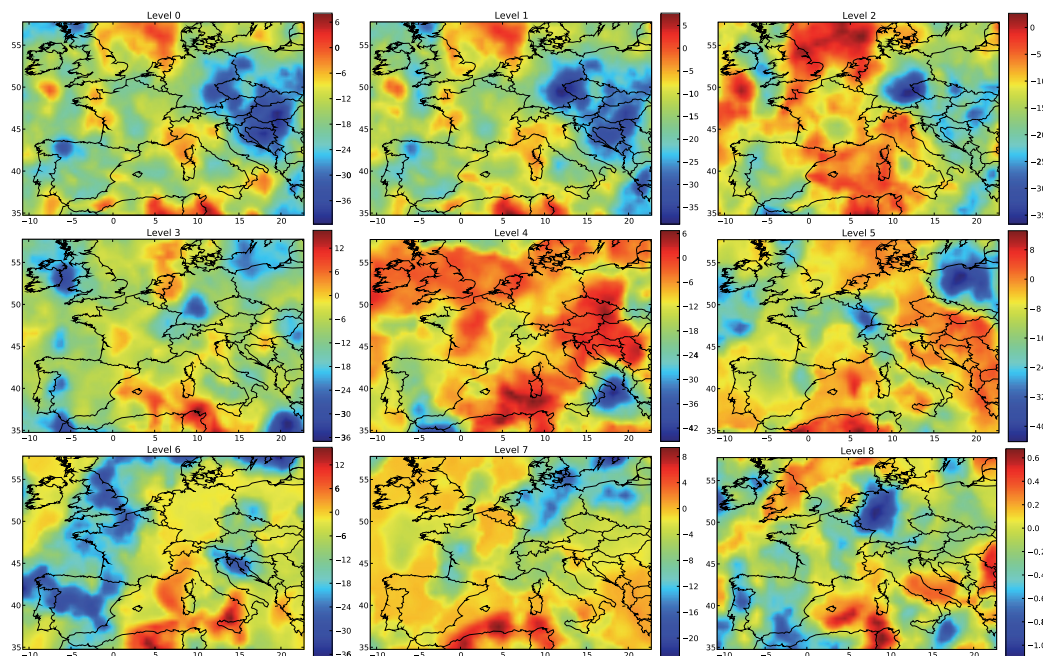
Fig. 5. Differences between "true" and perturbed PM$_{10}$ concentration at 00:00 UTC 15 July 2001 from first to last vertical level of the model. Differences (µg m^{-3}) vary from negative values in dark blue colour to positive values in dark red colour.

Title Page

Abstract | Introduction

Conclusions | References

Tables | Figures

◄◄ | ►►

◄ | ►

Back | Close

Full Screen / Esc

Printer-friendly Version

Interactive Discussion
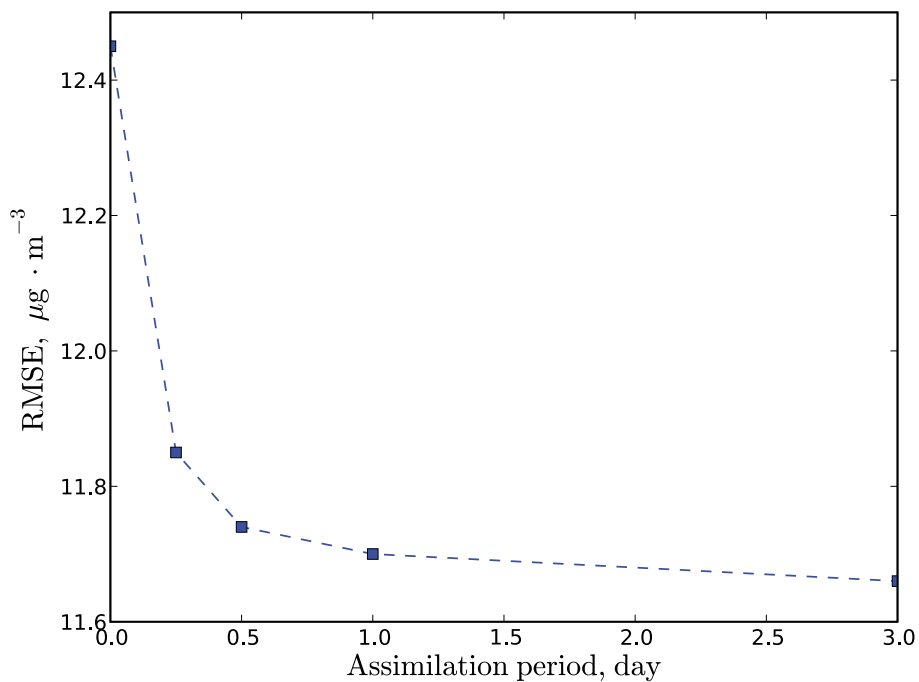
Fig. 6. RMSE (in $\mu g\, m^{-3}$) between the real observation and forecast concentrations from 18 July to 20 July against assimilation period (in days).
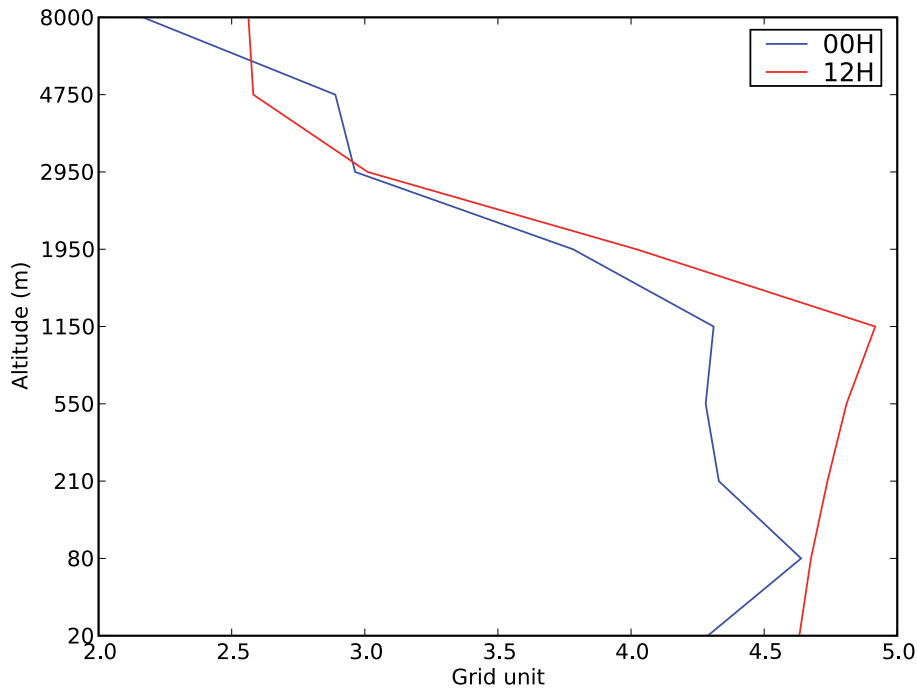
Fig. 7. The blue (resp. red) line shows the horizontal correlation length L_h at 00:00 UTC (resp. 12:00 UTC) versus altitude. Note that a grid unit is about 50 km.

Full Screen / Esc
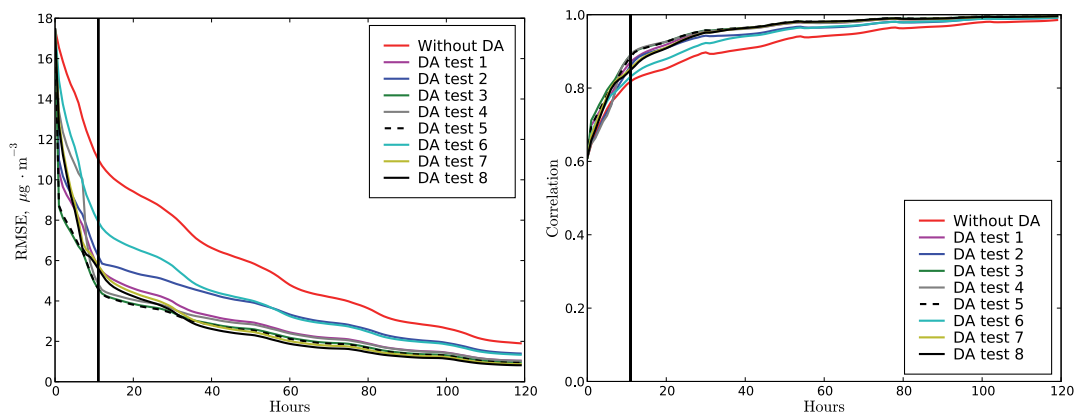
Fig. 8. Top (resp. bottom) figure shows the time evolution of the RMSE (resp. correlation) of PM_{10} averaged over the different DA tests from 15 July to 10 August 2001. The forecast is performed either without DA (red lines), or after AirBase DA or after column DA. Tests 1 to 5 correspond to AirBase DA, while tests 6 to 8 correspond to column DA. The correlation lengths are $L_h = 50\,km$ and $L_v = 1500\,m$ for test 1 (magenta lines), $L_h = 200\,km$ and $L_v = 250\,m$ for test 2 (blue lines), $L_h = 200\,km$ and $L_v = 1500\,m$ for test 3 (green lines), $L_h = 200\,km$ and $L_v = 50\,m$ in the nighttime and $L_v = 1500\,m$ in the daytime for test 4 (grey lines), $L_h = 400\,km$ and $L_v = 1500\,m$ for test 5 (black dashed lines), $L_h = 50\,km$ and $L_v = 0$ for test 6 (cyan lines), $L_h = 200\,km$ and $L_v = 0$ for test 7 (yellow lines), $L_h = 400\,km$ and $L_v = 0$ for test 8 (black lines).
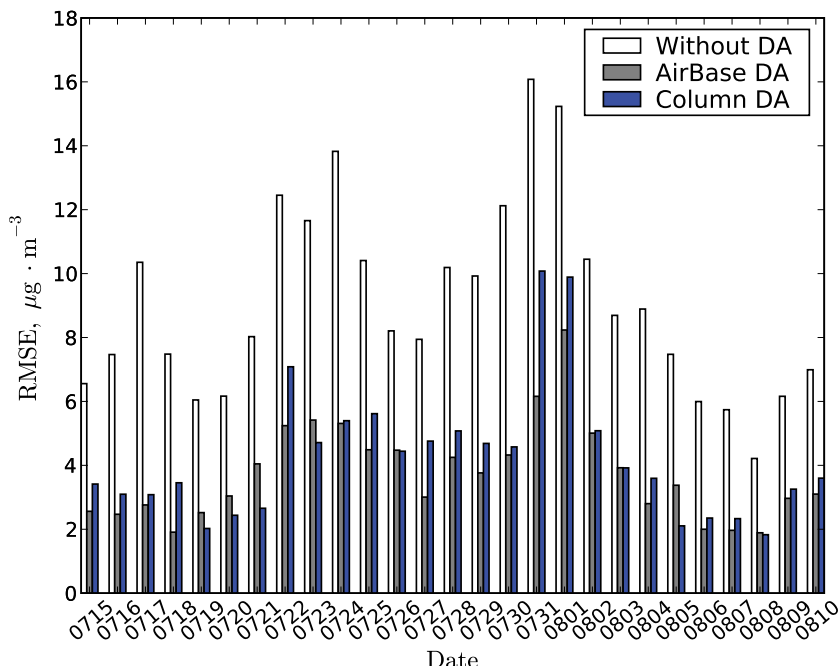
Fig. 9. RMSE (in $\mu g\,m^{-3}$) for PM_{10} one-day forecast without DA (white columns), with the Air-Base DA (grey columns) and with the column DA (blue columns).
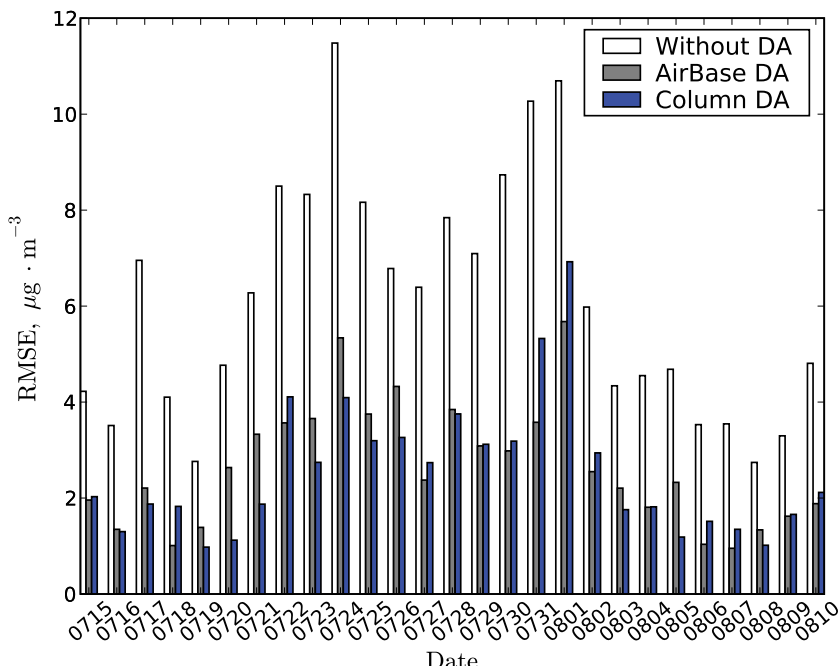
Fig. 10. RMSE (in µg m^{-3}) for PM$_{10}$ second forecast day without DA (white columns), with the AirBase DA (grey columns) and with the column DA (blue columns).

Full Screen / Esc
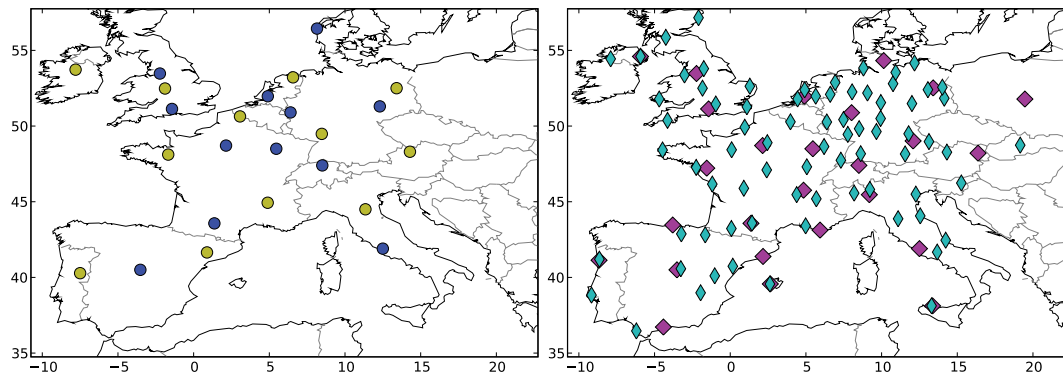
Fig. 11. Four potential lidar networks in Europe. The blue discs in the top figure show the locations of the reference lidar network. The yellow discs in the top figure show the locations of the lidar Network 1. The magenta diamonds in the bottom figure show the locations of the lidar Network 2. The cyan thin diamonds in the bottom figure show the locations of the lidar Network 3.
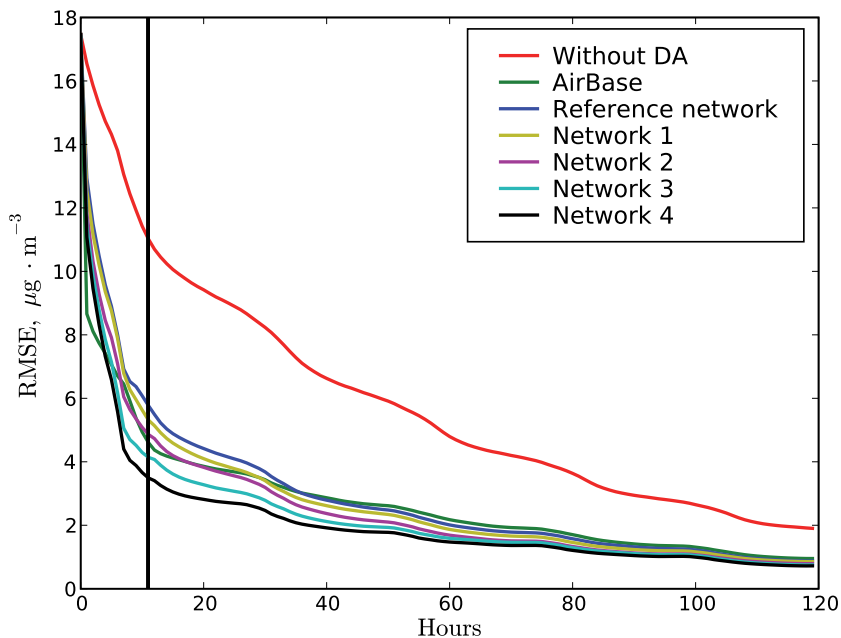
Fig. 12. Hourly evolution of the RMSE (in $\mu g\,m^{-3}$) of PM_{10} averaged over the different experiments from 15 July to 10 August 2001. The runs are performed without DA (red line), with Air-Base DA (green line), with the reference lidar network DA (12 stations, blue line), with Network 1 DA (12 stations, yellow line), with Network 2 DA (26 stations, magenta line), with Network 3 DA (76 stations, cyan line) and with Network 4 DA (488 stations, black line).
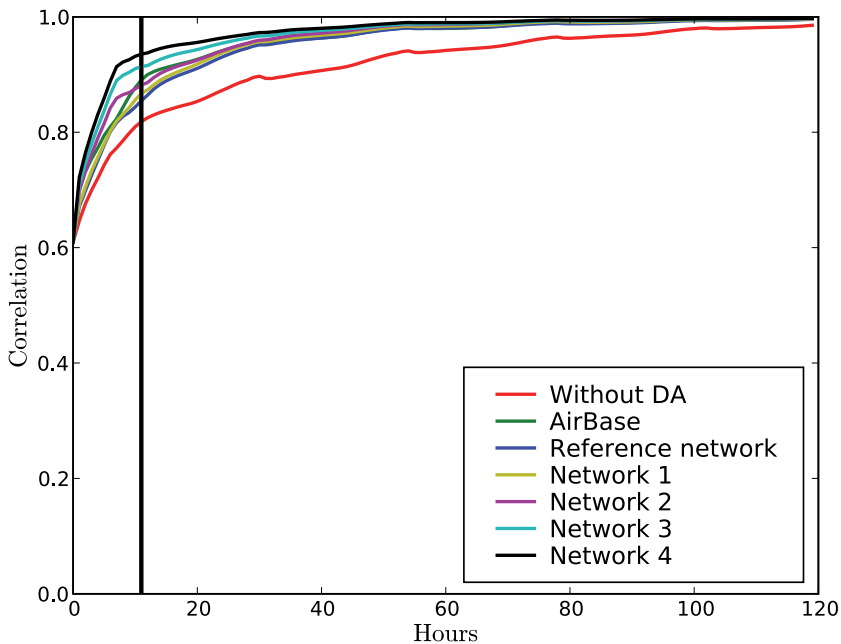
Fig. 13. Hourly evolution of the PM$_{10}$ correlation averaged over the different experiments from 15 July to 10 August 2001.The runs are performed without DA (red line), with AirBase DA (green line), with the reference lidar network DA (12 stations, blue line), with Network 1 DA (12 stations, yellow line), with Network 2 DA (26 stations, magenta line), with Network 3 DA (76 stations, cyan line) and with Network 4 DA (488 stations, black line).